

https://doi.org/10.1038/s40494-025-01966-7

# Color rendering evaluation model for lighting of traditional Chinese freehand brushwork paintings in museums

Check for updates

Zhuo Li<sup>1</sup>, Hu Wang<sup>1</sup>, Qinming Bai<sup>1</sup>, Kaida Xiao<sup>2</sup>, Yan Lu<sup>2</sup>, Lanlan Ma<sup>1</sup> & Rui Dang<sup>3</sup>

Traditional Chinese freehand brushwork paintings displayed in museums require lighting sources with high color rendering accuracy. However, due to their unique visual characteristics—such as low saturation, broad halos, and an emphasis on tonal gradation—existing general-purpose color rendering evaluation methods are often inadequate. In this study, a full-scale (1:1) replica of a traditional Chinese painting exhibition hall was constructed in a laboratory. Sixty representative spectral power distributions (SPDs) were used as lighting conditions, and four representative paintings were selected for evaluation. A color fidelity assessment was conducted with 34 participants. Five principal spectral components were extracted from each SPD and correlated with the fidelity evaluations using a neural network algorithm. Based on this analysis, a targeted color rendering evaluation model for lighting in traditional Chinese freehand brushwork painting exhibitions was developed. This model predicts the fidelity presentation value of a light source, with a validated average relative error of 9.7%.

Traditional Chinese paintings, as one of the most important exhibit types in museums, have display lighting that is a key focus and challenge in research: First, traditional Chinese paintings have a huge stock, with 560,000 existing pieces in China's collections, including numerous historical treasures of extremely high cultural and artistic value<sup>1</sup>, making them important components of world cultural heritage<sup>2</sup>. Second, due to their special material and craftsmanship characteristics, traditional Chinese paintings are classified by the International Commission on Illumination (CIE) as exhibits with the highest light sensitivity, being extremely prone to irreversible damage from optical radiation. For preservation needs, strict limits are imposed on the surface illuminance of these exhibits<sup>3-5</sup>. Meanwhile, as the architectural spaces for display are dim, viewing paintings in environments of low illuminance and high luminance contrast affects people's recognition of painting colors due to color visual-psychological effects. Third, traditional Chinese paintings are divided into two types by creative techniques: meticulous paintings and freehand brushworks. The latter, which use large color blocks for abstract expression<sup>6,7</sup>, —embodies the essence of traditional Chinese culture. It prioritize spiritual resemblance over physical likeness, featuring natural gradations in color shade, low overall saturation, and pronounced diffusion effects. Compared with meticulous paintings and Western oil paintings, freehand brushworks, deeply influenced by Taoist ideals of "simplicity is the greatest beauty" and Confucian values of "moderation and harmony," reflect more distinctive traditional Eastern aesthetic concepts<sup>8</sup>. In terms of color application and overall effect, it favors restraint and tends toward low-saturation tones, as shown in Fig. 1. Freehand brushwork painting is widely regarded as the most representative style of traditional Chinese painting. Display lighting, as a core factor determining their color quality, plays a crucial role in the authentic presentation of the paintings.

Based on the above characteristics and requirements of traditional Chinese painting lighting, how to evaluate the subjective perception of color fidelity of paintings by human eyes under different light sources is a key issue to be addressed. The current internationally adopted and latest light source color rendering evaluation method is the TM-30 light source color rendering evaluation method proposed by the Illuminating Engineering Society (IES). This method proposes a fidelity index  $(R_f)$ , gamut index  $(R_g)$ , and Color Vector Graphics (CVG) to determine color shifts of test light sources relative to reference sources<sup>9</sup>, playing a significant role in the lighting field<sup>10–12</sup>.

In recent years, researchers have studied the effects of  $R_f$  and  $R_g$  on color presentation for illuminated objects such as oil paintings  $^{13,14}$ . However, the optimal illuminance for oil paintings typically ranges between  $200-15,000 \, \mathrm{lx}^{15-20}$ , whereas due to material characteristics and preservation needs, the illuminance for traditional Chinese paintings is strictly limited to

Fig. 1 | Comparison of the traditional Chinese freehand brushwork painting and other paintings. a Chinese freehand brushwork painting: Dream Brush Blooming (Qian Song yan, modern times); b Meticulous painting: Spring Morning in the Han Palace (Qiu Ying, Ming Dynasty); c Western oil painting: Landscape painting (Albert Bierstadt, modern times).







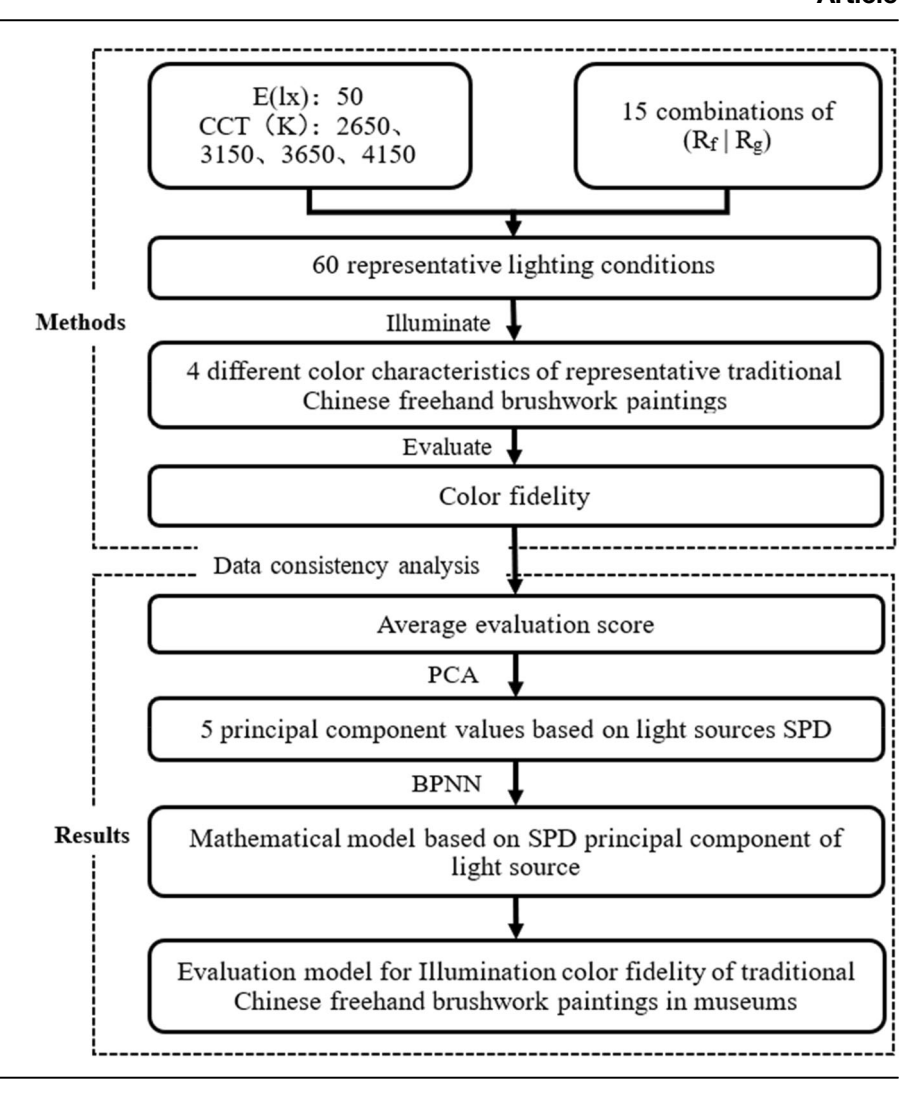
below 50 lx³-5. Additionally, viewer-preferred color temperatures for oil paintings fall between 3500 K-3700 K and 5100 K-5700  $K^{21,22}$ , while those for traditional Chinese paintings concentrate in the 3500–5000 K range²³. These differences indicate significant disparities in the display light environments between traditional Chinese paintings and oil paintings, making existing research results on oil painting lighting inapplicable directly to traditional Chinese paintings. Therefore, the research team previously analyzed studies on light source color rendering evaluation by Royer et al. 11,14 and conducted extensive research on the color rendering effects of traditional Chinese painting freehand brushwork lighting  $^{24-26}$ , identifying the influence patterns of  $R_f$  and  $R_g$  on color presentation in traditional Chinese freehand brushwork painting lighting. Meanwhile, it was discovered that even under the same  $R_f$  and  $R_g$  conditions, different light sources still lead to significant color perception differences  $^{11,14}$ .

This is because the IES TM-30 system is designed to evaluate the color rendering performance of light sources for all colors, which may have certain errors in applicability to specific special colors. First, the IES TM-30 evaluation method is established based on 105,000 object reflection spectra, encompassing spectral data from natural objects, industrial products, the Munsell color system, the Natural Color System (NCS), and the German Institute for Standardization (DIN), among others<sup>27</sup>. After screening, 99 standard color samples are retained. However, traditional Chinese freehand brushwork paintings rely on low-saturation water-based pigments and achieve abstract expression through large areas of color wash, resulting in gamut characteristics that differ significantly from conventional object colors<sup>6,7</sup>. To verify the coverage of these 99 standard color samples for traditional Chinese freehand brushwork painting colors, the typical colors of traditional Chinese freehand brushwork painting were identified through the following steps. First, drawing on the monographs Color in Chinese Painting-The Unfolding of the History of Chinese Painting Styles and Forms (Niu Kecheng)<sup>28</sup>, History of Chinese Painting (Pan Tianshou)<sup>29</sup>, and Research on Colors in Chinese Painting (Yu Fei'an)<sup>30</sup>, a comprehensive review of commonly used traditional pigments was conducted. Core pigments were then selected to define the primary hues, including cinnabar (red), ochre (brownish red/yellow), stone yellow (yellow), stone green (green, categorized into first, second, and third grades), and stone blue (blue). Additional inorganic mineral pigments such as head blue, second blue, chalk (white), lead white (white), clam powder (white), realgar (orange), and orpiment (lemon yellow), as well as organic plant- and animal-based pigments such as rattan (yellow), carmine (red), indigo (blue), and ink (black), were also included. Next, derivative hues were identified based on the blending of these pigments. According to traditional Chinese painting techniques, saturation gradients were adjusted by varying the amount of water added, while lightness gradients were achieved by incorporating clam powder (white) and different concentrations of ink (black). Following the principle of "covering as many colors as possible," eighteen representative traditional Chinese freehand paintings-each holding a canonical status in the history of Chinese painting and reflecting the characteristics of different schools, styles, and periods—were selected. From these, 304 typical color points were ultimately determined. Using an SRC-200S spectral colorimeter, we measured the relative spectral reflectance of these typical colors, which were then categorized into 82 typical colors through K-means clustering analysis. Comparisons revealed that TM-30 color samples only cover 37.8% of typical colors in Chinese paintings, indicating that the color samples used in TM-30 cannot fully represent the gamut characteristics of traditional Chinese freehand brushwork paintings. Second, due to preservation requirements, the lighting environment for traditional Chinese freehand brushwork paintings forms a distinctive highluminance-contrast setting—where the surface lightness of the paintings is relatively high while the ambient luminance is low. The IES TM-30 color rendering evaluation method, however, is based on the "average" environment type in CAM02, introducing limitations when applied to the special high-luminance-contrast lighting environments of museum galleries displaying traditional Chinese freehand brushwork paintings. Therefore, this study aims to develop a mathematical model based on the fundamental parameter of light sources—spectral power distribution (SPD)—to directly predict observers' perception of color fidelity in paintings, providing a new quantitative method for evaluating and selecting lighting sources for traditional Chinese paintings in museums.

However, the high-dimensional spectral features in the visible light band (380-780 nm), which include 81 variables (at 5 nm intervals), make direct analysis of the relationship between each wavelength and color fidelity excessively complex. To address such high-dimensional data analysis challenges, researchers have employed principal component analysis (PCA) to decompose spectral features 31-33 and reduce data dimensions. Through PCA, original high-dimensional variables are transformed into n principal components, with their importance and dimensionality reduction effectiveness evaluated by eigenvalues and cumulative contribution rates. An eigenvalue represents the variance of the original data explained by that principal component, while the cumulative contribution rate indicates the proportion of total variance explained by the first n principal components, measuring the retained information after dimensionality reduction. When eigenvalues exceed 1 or the cumulative contribution rate surpasses 90%<sup>34,35</sup>, it signifies greater data fluctuation and more information in that direction, indicating the principal component's significance. This approach satisfies dimensionality reduction needs while preserving key spectral features, providing reasonable input variables for subsequent modeling.

Meanwhile, the study's data exhibit multi-input single-output characteristics (n SPD principal components, 1 color fidelity score), necessitating a machine learning algorithm with strong nonlinear mapping capabilities. Traditional mathematically based modeling methods have notable limitations: linear regression cannot capture the complex relationship between spectral components and subjective perception, and support vector machines struggle to visualize input-output association paths in high-dimensional feature spaces. From a neurophysiological perspective, visual perception follows a hierarchical processing mechanism of "light stimulation—retinal photoreceptors—optic ganglion cells—lateral geniculate nucleus—visual cortex" 56–38. This nonlinear, hierarchical information transmission process fundamentally differs from linearly modeled mathematical assumptions. In contrast, bionic algorithms align better with visual perception mechanisms. Among these, swarm intelligence algorithms like particle swarm optimization focus on collective collaboration and lack direct

Fig. 2 | The technical roadmap.



relevance to individual visual pathways, while artificial neural network methods simulate neuron connections, with their hierarchical structure (input layer–hidden layer–output layer) closely matching visual conduction pathways. Specifically, backpropagation neural networks (BPNN) can optimize weights through gradient descent and are well-matched to the data characteristics and sample size, having been widely used in predictive modeling<sup>39–41</sup>. Thus, for this study, BPNN is the optimal algorithm choice that simultaneously satisfies data features, neural mechanisms, and computational efficiency.

To address the above issues, this study constructed a 1:1 scale simulated museum exhibition hall for Chinese paintings in the laboratory. In accordance with the lighting protection requirements for traditional Chinese paintings, 60 representative spectra were selected as experimental conditions by restricting the illuminance (E), correlated color temperature (CCT), fidelity index, and gamut index of light sources in the experimental cabinet. Four representative traditional Chinese freehand brushwork paintings with distinct color styles-cool-toned, warm-toned, mixed-color, and ink-dominatedserved as experimental samples. Thirty-four participants evaluated the color fidelity of these four types of freehand brushworks under 60 conditions in the simulated hall. The PCA was then applied to the light source SPD to obtain five principal component values characterizing the SPD. Finally, using BPNN data analysis, a mathematical model was established to predict observers' perception of painting color fidelity based on the principal components of light source SPD. The technical roadmap is shown in Fig. 2.

#### Methods

# **Experimental scene**

To conduct subjective evaluation experiments on the color fidelity of traditional Chinese freehand brushwork paintings, this research utilized the design recommendations for museum painting exhibition halls from the Architectural Design Dataset (3rd edition) and the index requirements outlined in the Code for Lighting Design of Museum (GBT 23863-2009). In the optical laboratory at Zhengzhou University, a 1:1 Chinese painting exhibition hall that represents the real light characteristics of museums was built as the experimental environment. The layout plan is shown in Fig. 3a. The dimensions of the experimental space are  $7.2 \times 4.65 \times 3.6$  m (length  $\times$ width × height), and the average reflectivity of the inner wall, ground, and ceiling are 0.6, 0.2, and 0.2, respectively. Six display cabinets were arranged within the experimental space. Cabinets No. 1 and No. 2 were used for subjective evaluations. Cabinets No. 3 to No. 6 were used for background ambiance creation. Both cabinets No. 1 and No. 2 were equipped with a THOUSLITE LED Cube lighting device with a luminous surface size of  $27 \times 27$  cm and a multi-channel spectral simulation system, which includes 14 narrowband LED channels (peak wavelengths covering 380-780 nm, as shown in Fig. 4. By independently controlling the LED channels' luminous intensity, the system can precisely generate any combination of SPD, fulfilling the needs of various experimental conditions. The device's luminous surface size was 27 × 27 cm. Cabinet No. 1 displayed the experimental light source, while Cabinet No. 2 simulated the reference light source. To minimize interference between light sources, a double layer of black light blocking cloth was placed between the two cabinets, as illustrated in Fig. 3b.

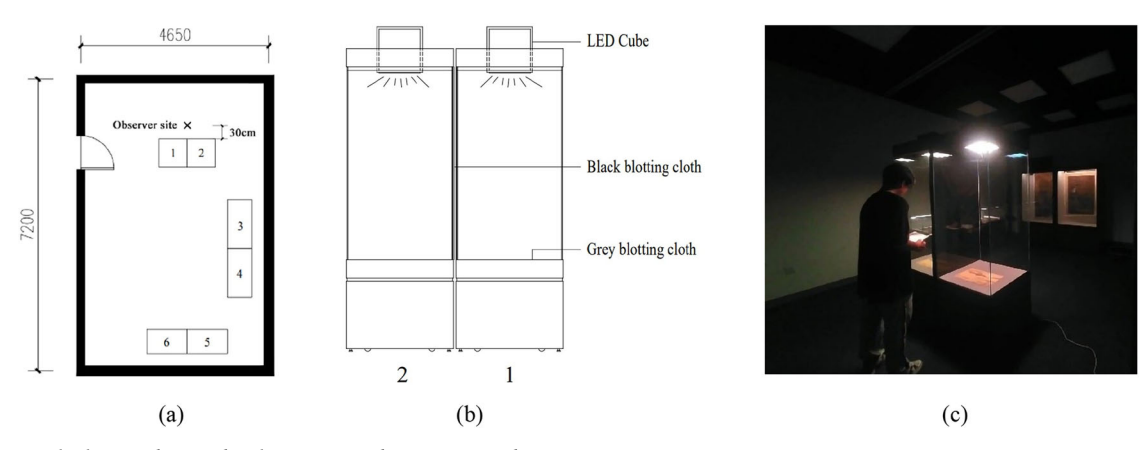


Fig. 3 | Experimental scheme. a layout plan; b Experimental scenario; c Evaluation experiment site.

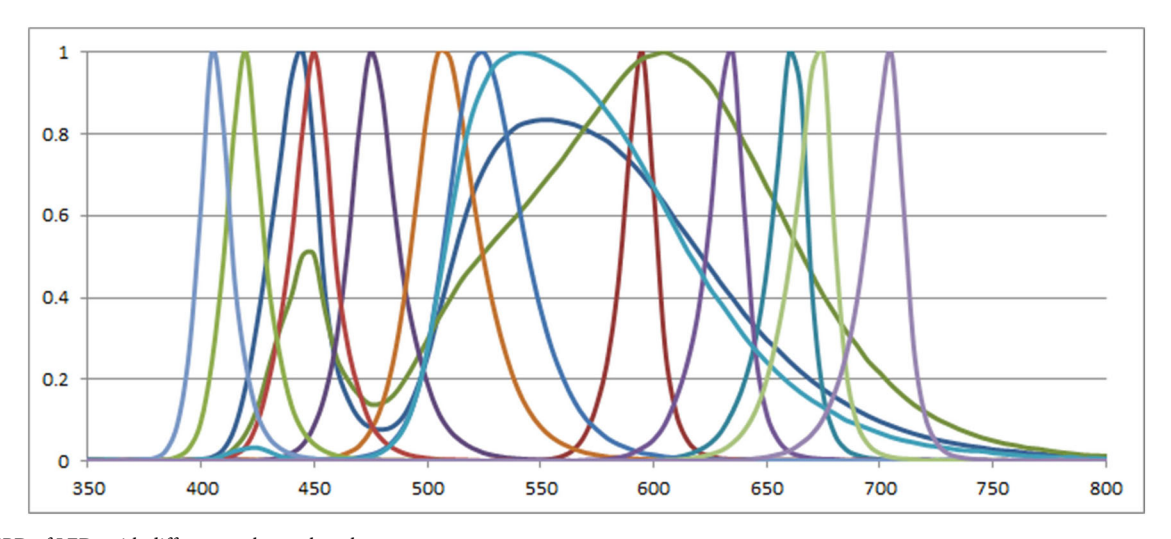


Fig. 4 | The SPD of LEDs with different peak wavelength.

The illuminance on the surface of the paintings in Cabinets No. 3 to No. 6 is set at  $50 \, \text{lx}$ , the CCT is  $3300 \, \text{K}$ , the average illuminance of the ground is  $10 \, \text{lx}$ , and the above lighting parameters remained constant during the experiment. The observer was instructed to stand at a fixed position to maintain a consistent viewing perspective. The painting samples were displayed flat within the cabinets, and the evaluation site is shown in Fig. 3c.

#### **Experimental conditions**

According to the illumination protection requirements for traditional Chinese paintings<sup>3–5</sup>, the surface illuminance of painting samples was set at 50 lx for this experiment. Based on the recommended ranges of CCT in CIE 157:2004<sup>4</sup> and ANSI/IES RP-30-20<sup>42</sup>, as well as the preservation requirements for traditional Chinese paintings<sup>42</sup>, four CCT values were selected: 2650 K, 3150 K, 3650 K, and 4150 K. Additionally, based on the distribution characteristics of the  $R_f$ -  $R_g$  space in TM-30-20<sup>43</sup>. These combinations were used to further screen the SPDs of the light sources. The  $R_f$  values of the light sources are uniformly distributed in the range of 65–100, and the  $R_g$  values are uniformly distributed in the range of 80–120. A total of 60 representative spectra were selected as experimental conditions, as shown in Fig. 5. In addition, Planckian radiations corresponding to the four CCT values were chosen as reference illuminants<sup>43</sup>. The parameters of the light sources are shown in Table 1.

## **Painting samples**

Traditional Chinese freehand brushwork paintings can be categorized into four types based on their color characteristics: cool colors, warm colors, mixed colors, and ink colors. According to the characteristics of color

classification, in this study, four representative paintings were selected respectively. The basic information and characteristics of the paintings are shown in Table 2. The four paintings included: Shenxiang Pavilion Peony Painting with mixed colors (Fig. 6a), Landscape Painting Album with cool colors (Fig. 6b), Six Scenes from the Song and Yuan Dynasties Album with warm colors (Fig. 6c), and Autumn Mountain Evening Mist Scroll, predominantly featuring ink colors (Fig. 6d). According to the museum-level digital replication technology. First, this research obtained high-definition electronic images (resolution ≥ 2880 × 1440 dpi) of four paintings from the official database of collected artworks and selected acid-free rice paper (pH 7.0-8.5) and silk fabric (warp/weft density: 120 × 80 threads/cm<sup>2</sup>) according to their substrate types to simulate the carrier characteristics of ancient paintings. Subsequently, professionals certified by the National Museum with cultural relic replication qualifications were commissioned to utilize an Epson Sure Color P9000 large-format printer. Through micro-piezoelectric printing technology, museumgrade ultra-high resolution outputs at 2880 × 1440 dpi were achieved, and human observation confirmed that the visual effects were completely consistent with those of the original artifacts. Therefore, this research employed two of the aforementioned museum-grade rice paper inkjet replicas (high-fidelity reproductions) as experimental samples, which were placed into Cabinet No. 1 (experimental condition group) and Cabinet No. 2 (reference light source group), respectively. To prove the difference in the main colors of the four paintings, the spectral reflection functions of the six main color points in the four paintings were measured by a spectral radiance

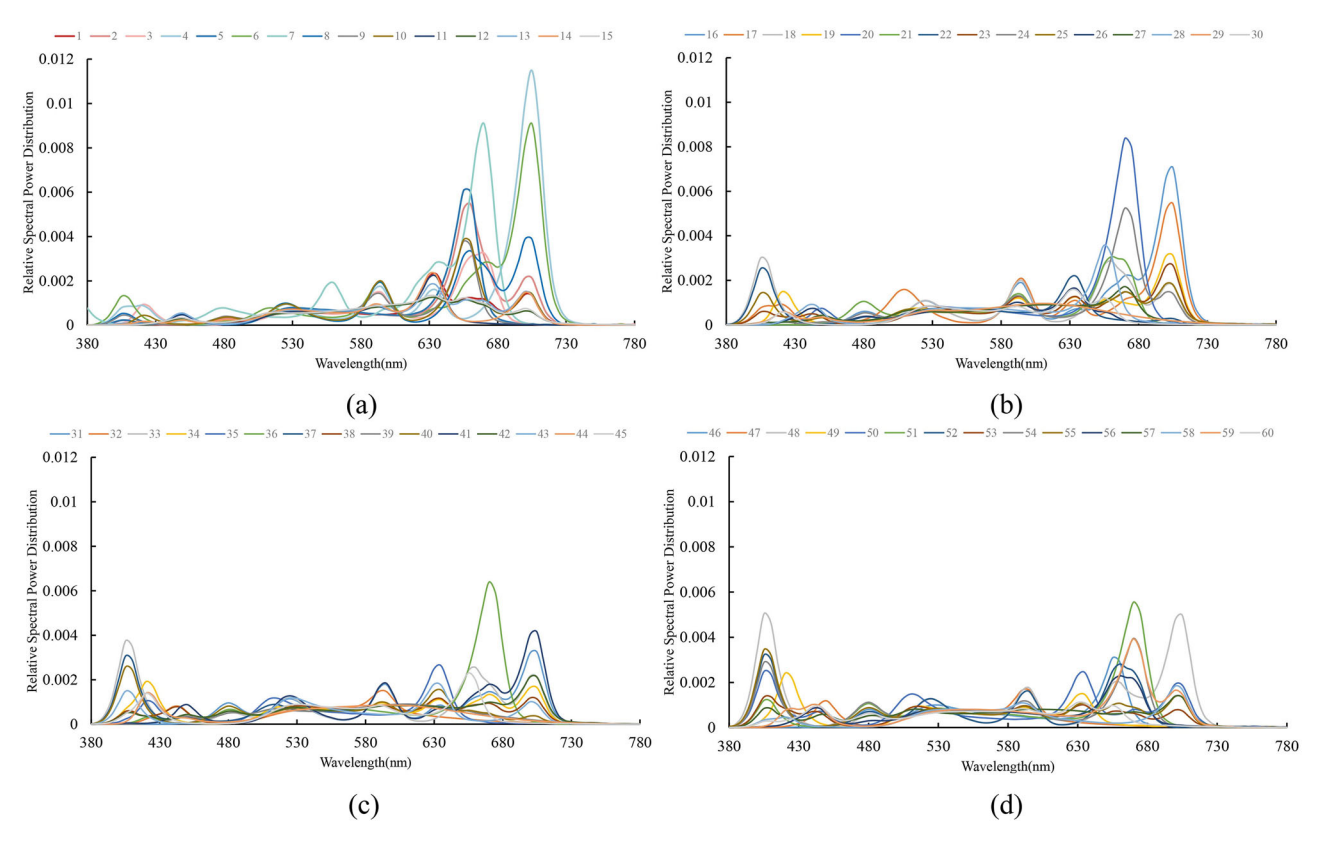


Fig. 5 | Relative SPD of the 60 experimental lighting conditions. a CCT = 2650 K; b CCT = 3150 K; c CCT = 3650 K; d CCT = 4150 K.

Table 1 | Lighting characteristics of the 4 reference illuminant conditions

E (lx)	CCT (K)	x	У	$R_f$	$R_g$
50.2	2647	0.4652	0.4135	96	103
50.1	3173	0.4180	0.4083	96	102
50.1	3697	0.3964	0.3897	95	100
50.0	4171	0.3746	0.3780	97	99

colourimeter (SRC-200S) under a CIE standard A light source (Fig. 6e). The corresponding color coordinates (L\*, a\*, and b\*) were calculated in the CIE 1976 LAB color space. Details are provided in Table 2.

# **Experimental process**

Thirty-four participants were selected based on the statistical characteristics of the data from the psychophysical experiments 19,44, half male and half female, who were students at Zhengzhou University. The age of the participants ranged from 18 to 26 years, with an average age of 22.6 years and a standard deviation of 2.8 years, which is slightly lower than the average age of real museum visitors. All participants passed the Ishihara color vision test and had normal corrected vision. The experiment was conducted daily from 8:30 to 11:30 in the morning and from 14:00 to 17:00 in the afternoon. Because the experiments were performed in a low illuminance light environment (≤50 lx) that simulated the high light sensitivity of cultural relic exhibition halls in museums, to reduce the experimental evaluation error caused by dark adaptation when the participants arrived at the experimental area from other bright areas, after entering the experimental area, the subjects are required to adapt for 15 minutes under a 50 lx neutral gray background (illuminated by a CIE D65 light source with  $L^* = 50$ ,  $a^* = 0$ , and b\*=0), during which the recorder described the experimental process. In the evaluation, a continuous scale was employed to assess the color fidelity of four traditional Chinese freehand brushwork paintings under different lighting conditions. This scale, shown in Table 3, is advantageous in studies involving individual differences<sup>45</sup>, enhancing the accuracy and generalizability of the results. The color fidelity represents the similarity between the overall color appearance of a painting under a given experimental condition and that under the reference light source.

To smoothly carry out the formal experiment and accurate understanding of color fidelity, pre-tests with four painting samples were conducted before the formal experiments. For each sample, 60 working conditions, as shown in Fig. 5, were established in the No. 1 display cabinet, with the corresponding reference illumination conditions set in the No. 2 display cabinet, as shown in Table 1. Initially, the first painting samples were placed in the No. 1 and No. 2 cabinets, and the experimental conditions were presented in a randomized order to familiarize participants with the environment. Each condition was displayed for 5 seconds<sup>46</sup>, and three conditions were randomly selected for scoring practice to ensure participants understood the evaluation requirements. In the formal experiment, 4 of the 60 working conditions were randomly repeated to analyze the reliability of participants' evaluations, resulting in a total of 64 conditions. To avoid the effect of visual fatigue on the experimental results, the 64 conditions were randomly divided into three groups. Each of the first two groups includes 26 working conditions, and the third group includes 12 working conditions. The duration of each condition was 25 seconds: participants rested with their eyes closed for 5 seconds based on voice prompts, in order to eliminate the influence of residual color vision, then had 15 seconds for visual adaptation and observation, followed by 5 seconds to record their evaluation. After completing one set of working conditions, take a 2-minute break. After the evaluation of each painting is finished, take a 5-minute break and conduct a dark adaptation recovery test. Using the first painting as an example, the evaluation process is shown in Fig. 7. Following the evaluation of the first painting, the remaining paintings were sequentially replaced, and this evaluation process was

Table 2 | Characteristics of painting samples

Title of Painting	Artist	Years	Collection Location	Color Characteristics	Picture Size	Main Color	[L*, a*, b*]
Shenxiang Pavilion Peony Painting	Wu Changshuo	1844- 1924	National Palace Museum, Taipei	Mixed colors	65*65 cm		[66,31 <b>–</b> 13], [79, –14, –2]
Landscape Painting Album	Shi Tao	1642–1707	The Palace Museum	Cool colors	20*30 cm		[76, -27, -11]
Six Scenes from the Song and Yuan Dynasties Album	Qiu Ying	1540– 1544	National Palace Museum, Taipei	Warm colors	30*45 cm		[68, 18, 19]
Autumn Mountain Evening Mist Scroll	Gao Kegong	1248- 1310	The Palace Museum	Ink colors	47*60 cm		[36, 16, 7], [68, 8, 3]

# **Results**

#### **Data consistency**

In order to analyze the reliability of the observers' data, in this research, Cronbach's alpha was applied to analyze intra-observer and inter-observer consistency. The results showed that the mean reliability coefficient (a) exceeded 0.95, indicating the reliability of the observer data were of high reliability and that all the evaluation data could be used for data analysis. After that, the arithmetic mean of the evaluation scores for the four painting types, as assessed by the 34 participants under identical working conditions, was calculated. Pearson correlation coefficients between the scores of the four painting types were then computed, as presented in Table 4. The results showed that the average Pearson correlation coefficient of the four paintings was 0.94 (p < 0.01), indicating a significant positive correlation. This suggests that differences in the color characteristics of the paintings do not considerably influence the evaluation of color fidelity under varying light sources. For the convenience of analysis, the average evaluation scores of the four painting types under identical experimental conditions were calculated to represent the overall color fidelity of traditional Chinese paintings. Therefore, for the convenience of analysis, the average evaluation values of the four painting types under the same experimental conditions were calculated to represent the color fidelity of traditional Chinese freehand brushwork paintings.

#### Principal components of light source SPD

The primary objective of this research is to establish a correlation model between the SPD of light sources and subjective color perception evaluations of traditional Chinese paintings. PCA was employed to reduce the dimensionality of high-dimensional spectral data. The visible light spectrum (380–780 nm) was sampled at 5 nm intervals, with each light source's SPD characterized by power values at 81 discrete wavelength points. PCA of 60 experimental SPD datasets indicated that the first five principal components exhibited eigenvalues exceeding 1. These components individually contributed 47.4%, 27.8%, 10.9%, 7.0%, and 2.8% to the variance, respectively, collectively explaining 95.9% of the total variance. This indicates that these components retained 95.9% of the original spectral information while preserving core spectral features and achieving dimensionality reduction. Based on the PCA results, a weight distribution plot of the five principal components across different wavelengths was generated, as shown in Fig. 8.

As shown in Fig. 8, the five principal components reveal the dominant roles of different spectral bands on light source characteristics through their weight coefficient distributions. Specifically, Principal Component  $X_1$  (variance contribution rate: 47.4%) reflects its spectral contributions in the 680–730 nm and 580–610 nm bands, corresponding to the light source's color reproduction capabilities for red and orange hues, respectively. Principal Component  $X_2$  (variance contribution rate: 27.8%) and Principal Component  $X_4$  (variance contribution rate: 7.0%) demonstrate their spectral contributions in the 640–700 nm and 640–670 nm bands, respectively, both associated with red hue reproduction capabilities. Principal Component  $X_3$  (variance contribution rate: 10.9%) indicates its spectral contribution in the 380–430 nm band, corresponding to blue hue reproduction capability, while Principal Component  $X_5$  (variance contribution rate: 2.8%)

reflects its spectral contribution in the 600–650 nm band, linked to the light source's orange-red hue reproduction capability.

Based on the spectral response characteristics characterized by the aforementioned principal components, the 81—dimensional original spectral data were reduced in dimension to 5 principal component values through linear combinations, thus providing interpretable input variables for subsequent perceptual models (calculation method detailed in Eq. (1)). Each principal component is defined as the sum of the products between the light source SPD and the eigenvector matrix (as shown in Table 5), where each column of the matrix represents a principal component (5 columns corresponding to the 5 principal components), and each element within the columns indicates the weight coefficient applied to the light source SPD.

$$X_n = \sum_{p=1}^{81} a_{np} \cdot \lambda_p \tag{1}$$

Where  $a_{np}(n=1\sim5,p=1\sim81)$  represents the p-th of the n-th principal component. A total of five principal components are present, with each principal component's eigenvector containing 81 weight coefficients. $\lambda_p$  represents the SPD value of the light source at the p-th wavelength point within the 380-780 nm range (sampled at 5 nm intervals). Through matrix operations, the SPD of each light source can be mapped into a vector composed of 5 principal component values  $[X]_{60} = [X_1, X_2, X_3, X_4, X_5]_{60}$ .

Based on the aforementioned methodology, this research calculated the principal component value matrix for 60 experimental conditions  $[X]_{60}$ , where each row corresponds to the 5 principal component values of a single light source. This result demonstrates that the high-dimensional spectral information of light source SPDs can be compressed into 5 principal component values, thus providing concise and highly interpretable input data for constructing subsequent perceptual models.

### The evaluation model

To establish a nonlinear mapping relationship between the SPD of light sources and color fidelity evaluations, this research constructs a mathematical model based on PCA dimensionality reduction results using a BPNN algorithm, which includes 5 input variables (principal component values) and 1 output variable (color fidelity score). To improve the model's prediction accuracy, the structure and parameters of the BPNN, as well as the data for model construction and validation, must be determined before using the BPNN algorithm to construct the model.

As shown in Fig. 9, the structure of the BPNN algorithm includes four parts: the input end, the hidden layer, the output layer, and the output end. Among them, the input end consists of the five normalized principal component values, denoted as  $x_i (i=1\sim5)$ . The hidden layer is denoted as  $N_j (j=1\sim n)$ , where j represents the number of units in the hidden layer. The internal parameters of the hidden layer include: the weight  $\omega_{ij}$ , which represents the connection strength between the input parameters  $x_i$  and the neurons  $N_j$  in the hidden layer; the constant  $b_{1j}$ , which represents the bias of the neurons  $N_j$  in the hidden layer. The output layer is denoted as N, and its internal parameters include: the weight

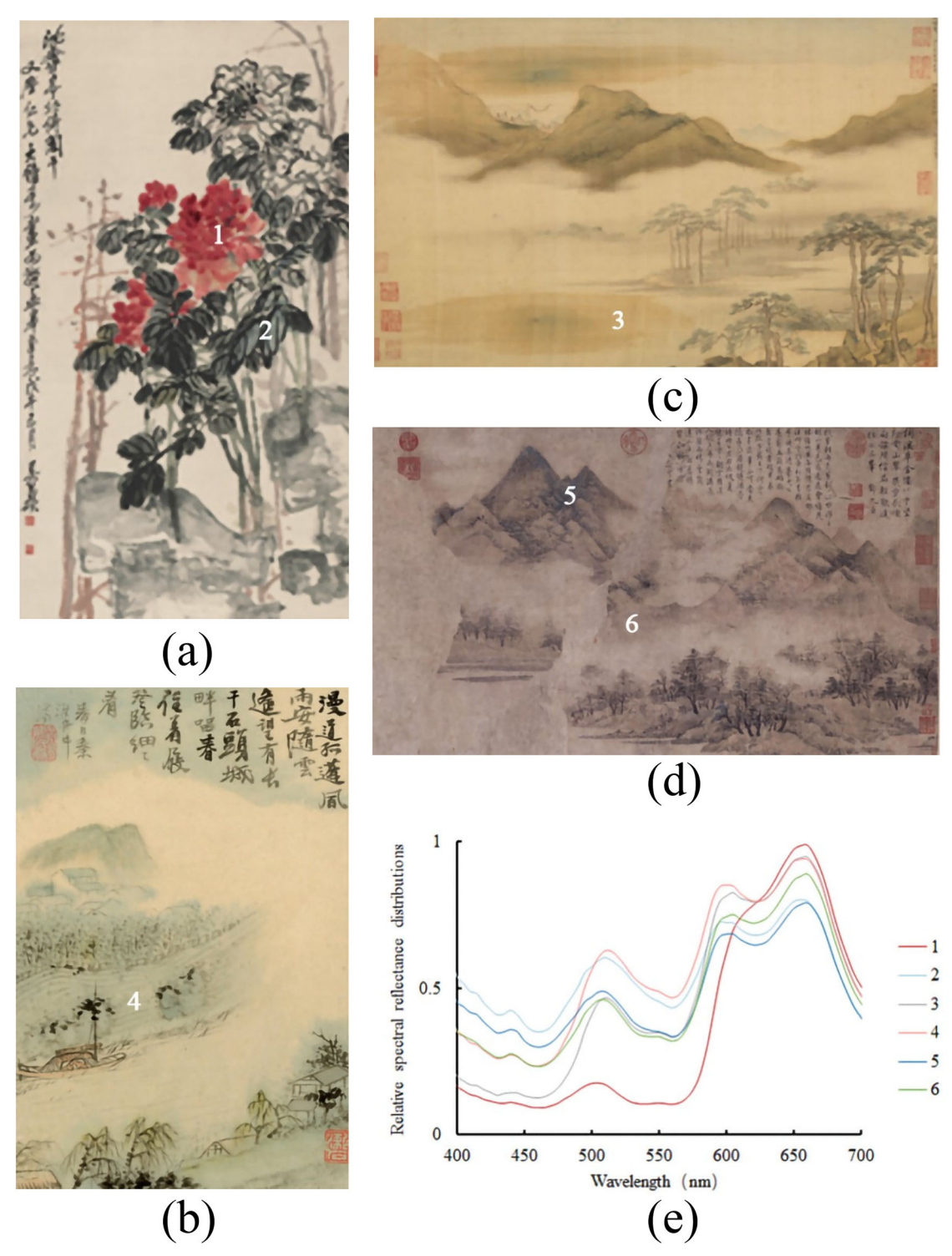


Fig. 6 | Painting samples used for the experiment. a "Shenxiang Pavilion Peony Painting"; b "Landscape Painting Album"; c "Six Scenes from the Song and Yuan Dynasties Album"; d "Autumn Mountain Evening Mist Scroll"; e The relative spectral reflectance distributions of 6 locations on the four paintings.

Table 3 | Evaluation scales and color fidelity ratings

Evaluation scale			
Evaluation score	[1,3)	[3,5)	[5,7]
Color fidelity grade	bad	normal	good

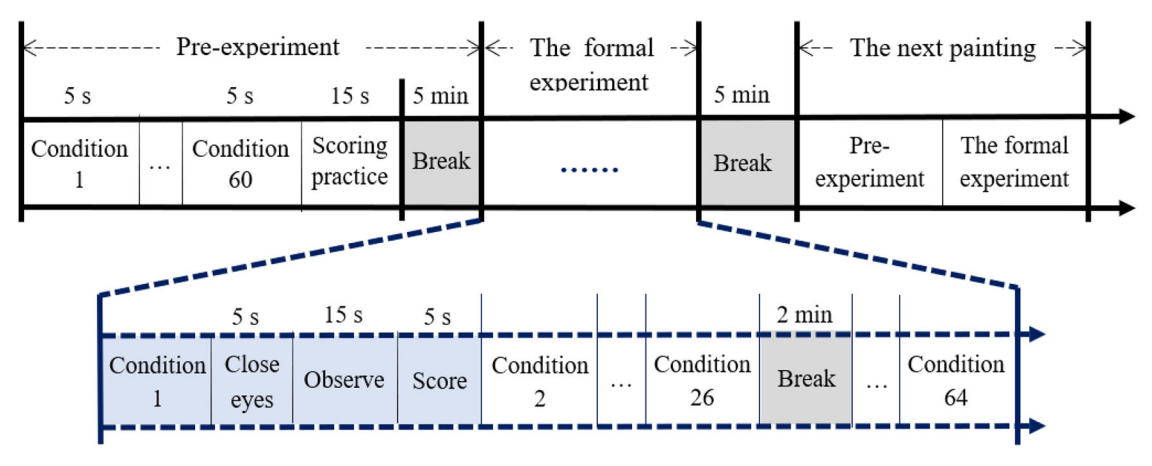


Fig. 7 | Time arrangement in subjective evaluation experiments.

Table 4 | The Pearson correlation between different types of painting

	Warm colors	Ink colors	Mixed colors
Cool colors	0.95*	0.94*	0.95*
Warm colors		0.92*	0.95*
Ink colors			0.91*

<sup>\*</sup>p < 0.01.

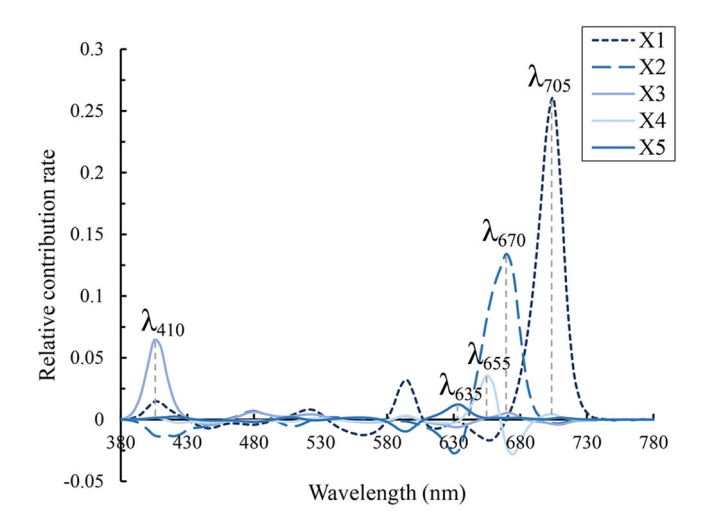


Fig. 8 | The weight distribution of the principal components of the spectrum at different wavelengths.

 $\omega_j$ , which represents the connection strength between the neurons in the hidden layer  $N_j$ , and the neurons N in the output layer; the constant  $b_2$ , which represents the bias of the neurons in the output layer. The output end, denoted as N, which represents the bias of the neurons in the output layer. The output end, denoted as y, represents the normalized predicted value of color fidelity.

Each part is connected through an activation function and a transfer equation. The activation function selected between the input end and the hidden layer is the Sigmoid function, as shown in Eq. (2):

$$f_1(x) = \frac{1}{1 + e^{-x}} \tag{2}$$

The transfer equation between the input end and the hidden layer:

$$H_{j} = f_{1} \left( \sum_{i=1}^{i=5} \omega_{ij} * x_{i} \right) - b_{1j}$$
 (3)

The activation function between the hidden layer and the output layer is Purelin, as shown in Eq. (4):

$$f_2(x) = x \tag{4}$$

The transfer equation between the hidden layer and the output layer:

$$y = \left(\sum_{j=1}^{j=n} \omega_j H_j\right) - b_2 \tag{5}$$

It can be seen from Eqs. (2) to (5) that the calculation equation used to predict the color fidelity is as follows:

$$y = \left\{ \sum_{j=1}^{j=n} \left[ \omega_j * \left( \frac{2}{1 + e^{-2((\sum_{i=1}^{j=5} \omega_{ij} * x_i) - b_{1j})}} - 1 \right) \right] \right\} - b_2$$
 (6)

After determining the BPNN architecture, it is necessary to define the model parameters, namely the convergence criteria and training parameters. This research selects the Levenberg-Marquardt algorithm with Mean Squared Error (MSE) as the loss function and the prediction correlation coefficient (R) of the entire dataset as the evaluation index for model prediction accuracy. A value of R > 0.8 indicates high prediction accuracy. The training parameters primarily include the number of hidden layers (j) and the Learning Rate of the algorithm, where the Learning Rate serves as a critical hyperparameter in the BPNN algorithm to control the adjustment step size of network weights and biases during each iteration. This research determines the hidden layer count and Learning Rate using a controlled variable comparison method, as shown in Fig. 10. Separately, relationships between the average MSE and average correlation coefficient R from five training sessions with the number of hidden layers and Learning Rate were established. Results indicate that the optimal training performance occurs when the number of hidden layers is 10 and the Learning Rate is 0.01. Collectively, the BPNN algorithm architecture and initial parameters adopted in this research are presented in Table 6.

Next, to avoid the over-fitting phenomenon when the BPNN algorithm trains the data and to effectively validate the obtained model later, this research divides the data of 60 experimental conditions and evaluations into

Table 5 | The eigenvector matrix of five principal components

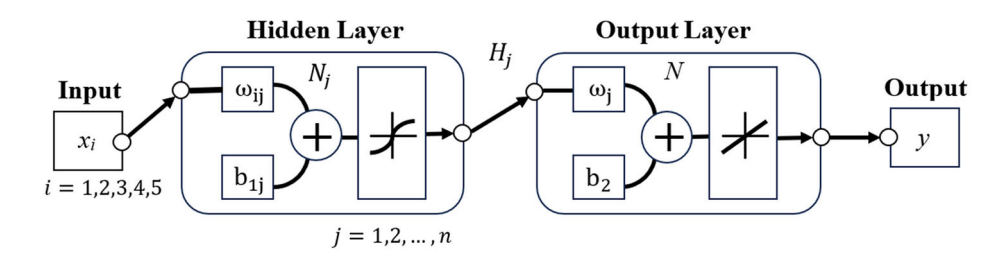
р	a <sub>np</sub>			p	a <sub>np</sub>						
	a <sub>1p</sub>	a <sub>2p</sub>	а <sub>3р</sub>	a <sub>4p</sub>	a <sub>5p</sub>		a <sub>1p</sub>	a <sub>2p</sub>	a <sub>3p</sub>	a <sub>4p</sub>	a <sub>5p</sub>
1	-0.0001	-0.0001	0.0019	-0.0001	0.0026	41	-0.0009	-0.0023	-0.0109	-0.0105	-0.0738
2	0.0009	-0.0006	0.0177	0.0003	0.0026	42	0.0262	-0.0048	0.0043	0.0104	-0.1736
3	0.0048	-0.0021	0.0669	0.0024	0.0080	43	0.0591	-0.0071	0.0238	0.0379	-0.2851
4	0.0127	-0.0052	0.1817	0.0048	0.0190	44	0.0706	-0.0087	0.0305	0.0480	-0.3135
5	0.0282	-0.0123	0.3877	0.0090	0.0436	45	0.0447	-0.0114	0.0150	0.0261	-0.2099
6	0.0426	-0.0206	0.5876	0.0086	0.0712	46	0.0083	-0.0160	-0.0084	-0.0055	-0.0727
7	0.0393	-0.0253	0.5412	-0.0015	0.0691	47	-0.0135	-0.0225	-0.0227	-0.0250	0.0213
8	0.0229	-0.0302	0.3144	-0.0242	0.0457	48	-0.0217	-0.0328	-0.0315	-0.0321	0.0913
9	0.0099	-0.0374	0.1435	-0.0472	0.0278	49	-0.0239	-0.0508	-0.0382	-0.0350	0.1801
10	0.0016	-0.0339	0.0532	-0.0503	0.0124	50	-0.0233	-0.0788	-0.0488	-0.0377	0.3083
11	-0.0038	-0.0229	0.0123	-0.0402	-0.0032	51	-0.0214	-0.1034	-0.0580	-0.0292	0.4426
12	-0.0084	-0.0157	-0.0083	-0.0368	-0.0168	52	-0.0177	-0.0860	-0.0536	0.0110	0.4581
13	-0.0126	-0.0117	-0.0265	-0.0393	-0.0300	53	-0.0148	-0.0132	-0.0350	0.0965	0.3113
14	-0.0148	-0.0075	-0.0390	-0.0408	-0.0372	54	-0.0111	0.0823	-0.0178	0.2161	0.1508
15	-0.0129	-0.0031	-0.0371	-0.0342	-0.0346	55	-0.0051	0.1856	-0.0026	0.3738	0.0647
16	-0.0088	0.0012	-0.0212	-0.0235	-0.0280	56	0.0051	0.2974	0.0103	0.5103	0.0317
17	-0.0055	0.0047	-0.0039	-0.0156	-0.0255	57	0.0209	0.3845	0.0130	0.3972	0.0369
18	-0.0040	0.0097	0.0114	-0.0125	-0.0294	58	0.0449	0.4408	0.0108	0.0122	0.0504
19	-0.0030	0.0178	0.0294	-0.0107	-0.0412	59	0.0718	0.4805	0.0108	-0.3278	0.0582
20	-0.0021	0.0264	0.0492	-0.0104	-0.0549	60	0.0894	0.4143	0.0027	-0.3989	0.0627
21	-0.0017	0.0302	0.0586	-0.0101	-0.0615	61	0.1090	0.2379	-0.0102	-0.2589	0.0516
22	-0.0008	0.0249	0.0530	-0.0083	-0.0506	62	0.1528	0.0870	-0.0169	-0.1099	0.0315
23	-0.0002	0.0141	0.0396	-0.0095	-0.0275	63	0.2331	0.0028	-0.0222	-0.0245	0.0188
24	0.0005	0.0039	0.0293	-0.0143	-0.0019	64	0.3516	-0.0449	-0.0301	0.0219	0.0152
25	0.0020	-0.0053	0.0248	-0.0199	0.0262	65	0.4910	-0.0782	-0.0375	0.0536	0.0174
26	0.0046	-0.0129	0.0247	-0.0227	0.0476	66	0.5394	-0.0896	-0.0451	0.0627	0.0315
27	0.0089	-0.0161	0.0298	-0.0190	0.0523	67	0.4052	-0.0711	-0.0438	0.0401	0.0432
28	0.0135	-0.0136	0.0377	-0.0064	0.0338	68	0.2060	-0.0382	-0.0300	0.0172	0.0316
29	0.0171	-0.0077	0.0420	0.0085	0.0069	69	0.0823	-0.0171	-0.0152	0.0054	0.0164
30	0.0162	-0.0016	0.0407	0.0163	-0.0071	70	0.0311	-0.0080	-0.0071	-0.0029	0.0050
31	0.0096	0.0021	0.0311	0.0143	-0.0039	71	0.0109	-0.0042	-0.0055	-0.0013	0.0013
32	-0.0001	0.0039	0.0170	0.0052	0.0086	72	0.0030	-0.0026	-0.0034	-0.0013	0.0014
33	-0.0091	0.0046	0.0047	-0.0045	0.0224	73	0.0011	-0.0017	-0.0010	-0.0023	-0.0003
34	-0.0164	0.0051	-0.0059	-0.0130	0.0319	74	0.0000	-0.0014	-0.0017	-0.0009	-0.0029
35	-0.0215	0.0047	-0.0138	-0.0196	0.0391	75	-0.0011	-0.0001	-0.0003	0.0012	-0.0016
36	-0.0253	0.0045	-0.0196	-0.0245	0.0435	76	-0.0005	-0.0007	-0.0001	-0.0023	-0.0005
37	-0.0280	0.0038	-0.0235	-0.0284	0.0436	77	-0.0004	-0.0006	0.0004	-0.0007	-0.0006
38	-0.0276	0.0024	-0.0249	-0.0292	0.0355	78	-0.0007	-0.0002	0.0005	0.0000	-0.0004
39	-0.0240	0.0011	-0.0243	-0.0281	0.0170	79	0.0004	0.0002	-0.0005	-0.0010	-0.0023
40	-0.0161	0.0000	-0.0208	-0.0216	-0.0151	80	0.0004	-0.0001	-0.0009	-0.0004	-0.0010
						81	-0.0001	0.0000	0.0003	-0.0002	-0.0014

a training set (70%), a validation set (15%), and a test set (15%) in proportion. The training set is the dataset used for training and learning. The BPNN learns the data features through the training set and generates a model for later prediction. The validation set is the dataset used for monitoring the model's performance. During the training process, the model adjusts its own parameters and hyperparameters through the validation set to avoid the situations of over-fitting or under-fitting. The test set is the dataset used for testing the final performance of the model. It does not overlap with the training set and the validation set,

and can evaluate the model's performance on unseen data, so as to judge whether the model is accurate enough<sup>40</sup>. Moreover, in order to avoid the errors caused by the order during data allocation, this research uses the Randperm function to randomly perturb the sampling order of each dataset, reducing the risk that the training order affects the training results<sup>47</sup>.

Prior to formal training, because different principal component values  $(X_1, X_2, X_3, X_4, X_5)$  may exhibit significant differences in units and numerical ranges due to spectral band energy variations (e.g., red light band energy is

Fig. 9 | The structure diagram of BPNN.



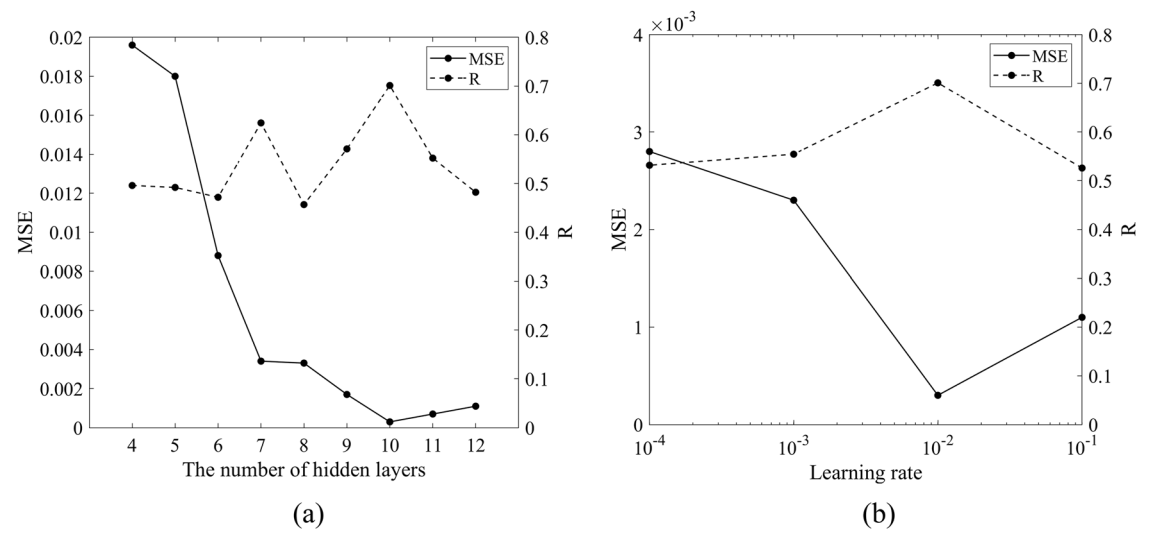


Fig. 10 | Parameter comparison of the BPNN algorithm. a The relationship between the number of hidden layers and the prediction accuracy of the model; b The relationship between the learning rate and the prediction accuracy of the model.

generally higher than blue light band energy), this research performs normalization on these values. They are linearly mapped to the [0-1] interval and denoted as  $x_1, x_2, x_3, x_4, x_5$ . The normalization calculation equation is as follows:

$$x = \frac{X - X_{min}}{X_{max} - X_{min}} \tag{7}$$

Here, x represents the normalized value, X denotes the non-normalized input value,  $X_{min}$  is the minimum value of the non-normalized data, and  $X_{max}$  is the maximum value of the non-normalized data. Based on the architectural configuration of the BPNN algorithm, parameter selection, and dataset allocation method described above, this research trained the

16th generation, and Fig. 11b indicates that the correlation coefficient R between the model's predicted values and target values was 0.85 (R > 0.8), confirming the network's high prediction accuracy. The internal architectural parameters of the trained model are listed in Table 7.

In order to quantify the effect of illumination light source SPD on the perceived color fidelity of traditional Chinese freehand brushwork paintings, this research first obtained the five principal components representing the light source's SPD through PCA. Subsequently, an evaluation model for the color fidelity of illumination of traditional Chinese freehand brushwork paintings in museum was developed using BPNN algorithm.

Substituting the optimal  $\omega_{ij}$ ,  $b_{1j}$ ,  $\omega_{j}$ ,  $b_{2i}$  parameters into Eq. (6), the mathematical matrix model for calculating the perceived color fidelity of traditional Chinese freehand brushwork paintings in museums under different lighting conditions can be obtained, as shown in Eq. (8).

$$y = \begin{bmatrix} -1.919 & 0.862 & 0.581 & 0.546 & -2.663 \\ -1.292 & 1.460 & 3.164 & 0.617 & -1.705 \\ -1.653 & 0.974 & 0.432 & -0.718 & 0.658 \\ -0.544 & 0.609 & -1.364 & -1.325 & 0.020 \\ 2.229 & 4.043 & -3.787 & -3.756 & -3.535 \\ -0.616 & 0.882 & 2.126 & -0.404 & -4.727 \\ 0.484 & -1.092 & -1.144 & -2.124 & 2.359 \\ -1.309 & 0.084 & 1.874 & -1.802 & -1.318 \\ -1.082 & 0.673 & 0.465 & 1.550 & 0.213 \\ 0.536 & -1.383 & -1.119 & -0.721 & -1.077 \end{bmatrix} \cdot \begin{bmatrix} x_1 \\ x_2 \\ x_3 \\ x_4 \\ x_5 \end{bmatrix} - \begin{bmatrix} 2.011 \\ 2.778 \\ 1.594 \\ 1.000 \\ 2.028 \\ -0.518 \\ -0.513 \\ -0.610 \\ -1.575 \\ 2.087 \end{bmatrix} \cdot \begin{bmatrix} -0.887 \\ -1.248 \\ 1.255 \\ -0.588 \\ 0.716 \\ -2.147 \\ -1.896 \\ 1.845 \\ -0.107 \\ 0.372 \end{bmatrix} - [0.174]$$
 (8)

color fidelity evaluation data of traditional Chinese freehand brushwork paintings. The training results are presented in Fig. 11. It is shown in Fig. 11a that the network's structural parameters reached their optimal state at the

Where y is the normalized color fidelity perceived prediction value and  $x_1, x_2, x_3, x_4$  and  $x_5$  are the normalized 5 principal component values. When using the model to evaluate the color fidelity of a light source, first, the

five principal component values of the light source are calculated according to Eq. (1) and the eigenvector matrix in Table 5, including  $X_1, X_2, X_3, X_4, X_5$ , and then the normalized parameters  $x_1, x_2, x_3, x_4$  and  $x_5$  of the five principal component values are substituted into Eq. (8) to obtain the normalized color fidelity prediction value y. The predicted color fidelity is obtained via inverse normalization of y, and the color fidelity level corresponding to the predicted color fidelity value can be obtained by comparison Table 3. With this approach, the perceived color fidelity of lighting sources for traditional Chinese freehand brushwork paintings in museums can be quantitatively calculated and evaluated.

## **Discussion**

The regression results reflect the high prediction accuracy of the network. To further verify the accuracy of the model in calculating the color fidelity of traditional Chinese freehand brushwork paintings in museums, a test set not involved in model construction was selected for validation analysis. Specifically, the mean relative error  $(\delta)$  between the experimental evaluation scores F' of the test set light sources and the model-predicted values F was calculated using the following equation:

$$\delta = \left| \frac{(F' - F)}{F'} \right| \times 100\% \tag{9}$$

Table 6 | Parameter Settings of the Model

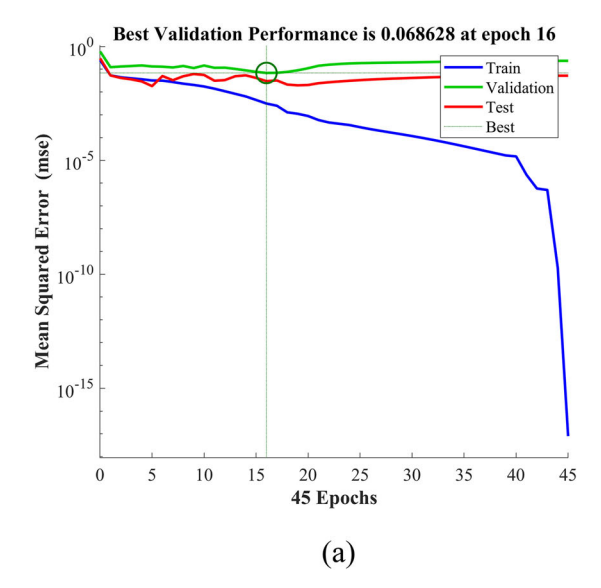
Parameter	Value
Number of neurons in the input layer	5
Number of neurons in the hidden layer	10
Number of neurons in the output layer	1
Learning rate	0.01
Number of iterations	100
Number of cross-validation times	100
Activation function between the input layer and the hidden layer	Sigmoid
Activation function between the hidden layer and the output layer	Purelin
Training function	Levenberg-Marquardt
Model evaluation metric	R

From the calculation results (Table 8), the mean relative error between the model's color fidelity prediction results and actual subjective evaluations was 9.7%. Considering the practical application scenario, this error range is acceptable, indicating that the model's predicted data aligns with actual subjective evaluations and its prediction results for color fidelity are satisfactory.

Additionally, to enable model users to conveniently select appropriate light sources based on prediction levels, this research calculated the color fidelity model prediction values for 60 working conditions using the above method. These values were compared with experimental evaluation values to determine the accuracy rate of the model in predicting the perceived color fidelity levels of museum lighting sources for traditional Chinese freehand brushwork paintings. Here, the accuracy rate is defined as the percentage of correct predictions for a given dataset. Under three color fidelity levels, the number of model prediction values matching the true evaluation results is presented in Table 9. As shown in Table 9, among 60 working conditions, 53 model prediction values were consistent with the true evaluation values, indicating that the model achieved an 88.3% accuracy rate in predicting the perceived color fidelity levels of traditional Chinese freehand brushwork paintings.

It is worth noting that the experimental conditions used in color fidelity evaluation experiments in this research are limited, and the participants are students aged 18-26 years (M=22.6, SD=2.8), which presents a discrepancy compared to the average age of museum visitors (18–35 years). Therefore, future research plans include two components: (1) Adjust the light source SPD, increase the number of experimental conditions, and revise and refine the model; (2) Expand the participant pool to include individuals of varying ages, genders, and occupations to conduct a study on differences in perceived color fidelity of traditional Chinese freehand brushwork paintings in museums across different populations. Additionally, correlation coefficient values may be revised based on data obtained from future experiments.

In this research, principal component analysis was employed to demonstrate that the spectral power distribution of light sources can be characterized by five principal component values. Based on this finding, an evaluation model for assessing the color fidelity of illumination in traditional Chinese freehand brushwork paintings was developed. To apply this model, the SPD of the light source is first measured using a spectrometer. The five principal component values of the SPD are then calculated through the eigenvector matrix and input into the model to derive the predicted color fidelity value of traditional Chinese freehand brushwork



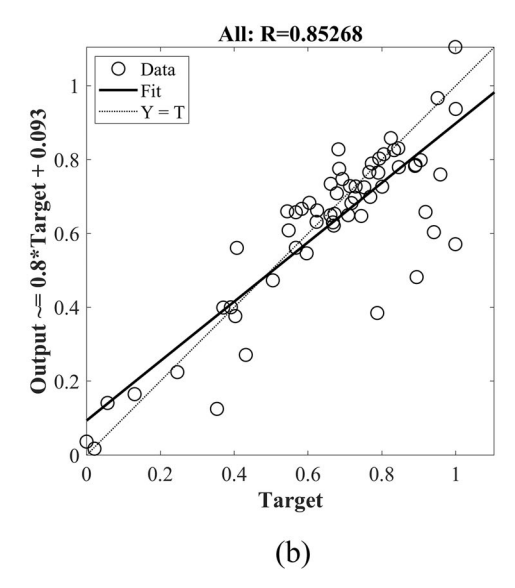


Fig. 11 | Training results. a The trend of the MSE for the three datasets; b The regression analysis of the model.

Table 7 | The structural parameters of the model

	ω <sub>ij</sub>			b <sub>1j</sub>	ω <sub>j</sub>	b <sub>2</sub>		
	ω <sub>1j</sub>	ω <sub>2j</sub>	ω <sub>3j</sub>	$\omega_{4j}$	ω <sub>5j</sub>			
Neuron_N <sub>1</sub>	-1.919	0.862	0.581	0.546	-2.663	2.011	-0.887	0.174
Neuron_N <sub>2</sub>	-1.292	1.460	3.164	0.617	-1.705	2.778	-1.248	
Neuron_N <sub>3</sub>	-1.653	0.974	0.432	-0.718	0.658	1.594	1.255	
Neuron_N <sub>4</sub>	-0.544	0.609	-1.364	-1.325	0.020	1.000	-0.587	
Neuron_N <sub>5</sub>	2.229	4.043	-3.787	-3.756	-3.535	2.028	0.716	
Neuron_N <sub>6</sub>	-0.616	0.882	2.126	-0.404	-4.727	-0.518	-2.147	
Neuron_N <sub>7</sub>	0.484	-1.092	-1.144	-2.124	2.359	-0.513	-1.896	
Neuron_N <sub>8</sub>	-1.309	0.084	1.874	-1.802	-1.318	-0.610	1.845	
Neuron_N <sub>9</sub>	-1.082	0.673	0.465	1.550	0.213	-1.575	-0.107	
Neuron_N <sub>10</sub>	0.536	-1.383	-1.119	-0.721	-1.077	2.087	0.372	

Table 8 | Relative Errors between the Prediction Results of the Test Set and the Experimental Evaluation Results

ID	Experimental evaluation results (F')	Prediction results (F)	Relative error(δ)
1	2.09	1.97	5.4%
2	4.79	4.79	0%
3	4.59	4.43	3.4%
4	4.52	4.59	1.7%
5	2.64	1.46	4.49%
6	3.84	4.27	11.3%
7	3.65	3.97	8.6%
8	4.29	4.04	5.9%
9	4.36	4.84	10.8%

Average: 9.7%.

Table 9 | Number of 60 working condition model predictions that meet the evaluation value

	good	normal	bad
Evaluation value	13	37	10
Predicted value	10	34	9

paintings under the specific light source. By comparing the predicted value with Table 3, the corresponding color fidelity grade can be determined, thus realizing the quantitative calculation and evaluation of color fidelity for museum lighting of traditional Chinese freehand brushwork paintings. This model can quantitatively predict observer-perceived color fidelity of traditional Chinese freehand brushwork paintings illuminated by different SPDs at an illuminance of 50 lx, addressing the critical demand for accurate color fidelity in traditional Chinese freehand brushwork painting conservation. This research has taken an important step forward in the research on achieving optimal museum lighting for Chinese paintings. Additionally, the research methodologies and mathematical model established in this research provide valuable references for lighting studies on colored cultural relics in museums, serve as a basis for formulating museum lighting standards, and offer practical guidance for exhibition lighting design in museum settings.

#### Data availability

The datasets analysed during the current study are available from the corresponding author on reasonable request.

Received: 2 January 2025; Accepted: 23 July 2025; Published online: 29 August 2025

#### References

- National Cultural Heritage Administration. The 13th Five-Year Plan for the Development of National Cultural Relics[Z]. (2017).
- Administration N. C. H. Nearly one billion people enter the museum [EB/OL]. http://www.sach.gov.cn/art/2019/1/10/art\_1027\_153349. html (2019).
- Pinto, P. D., Linhares, J. M. M. & Nascimento, S. M. C. Correlated color temperature preferred by observers for illumination of artistic paintings. J. Opt. Soc. Am. A Opt. Image Sci. Vis. 25, 623–630, https:// doi.org/10.1364/JOSAA.25.000623 (2008).
- C.I. de L'Eclairage, CIE 157: 2004 Control of damage to museum objects by optical radiation, Vienna, Austria: CIE, 2004.
- Standardization Administration of the People's Republic of China.
  Code for Lighting Design of Museums [S] (GB/T 23863–2024), (China Standards Press, Beijing, 2024).
- Gao, F. et al. Traditional Chinese painting classification based on painting techniques. *Chin. J. Comput.* 40, 2871–2882 (2017).
- Hong, D. On the concept of 'freehand'- meticulous painting and freehand brushwork painting. Art. Lit. Masses 15, 116 (2010).
- Dang, R. et al. Chromaticity shifts due to light exposure of inorganic pigments used in traditional Chinese painting. *Light. Res. Technol.* 49, 818–828, https://doi.org/10.1177/1477153516644866 (2017).
- Royer, M. P. Tutorial: background and guidance for using the ANSI/ IES TM-30 method for evaluating light source color rendition. LEUKOS J. Illuminat. Eng. Soc. North Am. 1–41. https://doi.org/10. 1080/15502724.2020.1860771 (2021).
- Boyce, P. R. & Stampfli, J. R. LRT Digest 3: new colour metrics and their use. *Light. Res. Technol.* 51, 657–681, https://doi.org/10.1177/ 1477153519850006 (2019).
- Royer, M., Wilkerson, A. & Wei, M. Human perceptions of colour rendition at different chromaticities. *Light. Res. Technol.* 50, 965–994, https://doi.org/10.1177/1477153517725974 (2018).
- Innes, M. Correspondence: In support of the IES method of evaluating light source colour rendition. *Light. Res. Technol.* 47, 1029–1034, https://doi.org/10.1177/1477153515617392 (2015).
- Feltrin, F. et al. Impact of illumination correlated color temperature, background lightness, and painting color content on color appearance and appreciation of paintings. *Leukos* 16, 25–44, https://doi.org/10.1080/15502724.2018.1522261 (2020).
- Royer, M. P. et al. Human perceptions of colour rendition vary with average fidelity, average gamut, and gamut shape. *Light. Res. Technol.* 49, 966–991, https://doi.org/10.1177/1477153516663615 (2016).

- Luo, H. W. et al. Using LED technology to build up Museum lighting environment. in *Proc. 12th Conference of AIC Colour, Tyne, UK*, pp. 1757–1760, (2013).
- Zhai, Q., Luo, M., Liu, X. The impact of illuminance and colour temperature on viewing fine art paintings under LED lighting. *Light. Res. Technol.* 1477153514541832. https://doi.org/10.1177/ 1477153514541832 (2014).
- Zhai, Q. Y., Luo, M. R. & Liu, X. Y. The impact of LED lighting parameters on viewing fine art paintings. *Light. Res. Technol.* 48, 711–725, https://doi.org/10.1177/1477153515578468 (2016).
- F. Szabó, R. Kéri, P. Csuti. The preferred conditions of LED lighting for fine art paintings: the influence of illuminance level and correlated colour temperature. in 1st International Museum Lighting Symposium, (London), pp. 50–52 (2017).
- Wei, M., Bao, W. & Huang, H. P. Consideration of light level in specifying light source color rendition. *LEUKOS* 16, 55–65, https://doi.org/10.1080/15502724.2018.1448992 (2020).
- Bao W., Wei M. Change of Gamut Size for Producing Preferred Color Appearance from 20 to 15000 lux (Taylor & Francis, 2021). https://doi. org/10.1080/15502724.2019.1587621.
- Illuminating Engineering Society. ANSI/IES RP-30-20, Recommended Practice Lighting Museums[S], (Illuminating Engineering Society, New York, 2020).
- Nascimento, S. M. C. & Masuda, O. Best lighting for visual appreciation of artistic paintings—experiments with real paintings and real illumination. J. Opt. Soc. Am. A Opt. Image Sci. Vis. 31, A214, https://doi.org/10.1364/JOSAA.31.00A214 (2014).
- Li, Z. et al. Indicators for lighting Chinese paintings in museums based on the protection standards and color preferences. *Energy Build.* 299, 9, https://doi.org/10.1016/j.enbuild.2023.113610 (2023).
- Dang, R., Wang, S., Sun, X., Tang, M. & Yang, D. The mathematical model for colour preference in Chinese painting within museum lighting environments. *Color. Technol.* 141, 238–248, https://doi.org/ 10.1111/cote.12778 (2025).
- Dang, R. et al. The influence rules of illumination light source color parameters on the color trueness of chinese painting and its mathematical model. *Leukos*. 1–11. https://doi.org/10.1080/ 15502724.2025.2461300 (2025).
- Dang, R. et al. Data-based modeling of the light source color indicators on the Color Discrimination Index of the Forbidden City typical color paintings. Opt. Express 33, 8065–8082 (2025).
- David, A. et al. Development of the IES method for evaluating the color rendition of light sources. Opt. Express 23, 15888–15906, https://doi. org/10.1364/OE.23.015888 (2015).
- Niu, Kecheng. Chinese Painting in Colors: The Historical Development of Chinese Painting Styles and Forms (Hunan Fine Arts Publishing House, 2002).
- 29. Pan, T. A History of Chinese Painting (Unity Press, 2011).
- Yu, F. & Liu, L. Research on the Colors of Chinese Paintings (Beijing United Publishing Co, 2013).
- Rundquist, D. C. & Di, L. Band-moment analysis of imagingspectrometer data. 55, 3–208 (1989).
- Shams-Nateri, A. et al. Colorimetric Study on Polyamides Dyeing With Weld and Pomegranate Peel Natural Dyes. *Cloth. Text. Res. J.* 32, 124–115, https://doi.org/10.1177/0887302X14525658 (2014).
- Das, A. & Mandal, M. Study of color degradation in package prints: Analyzing kinetics with principal component analysis. *Color Res. Appl.* 49, 15, https://doi.org/10.1002/col.22924 (2024).
- Kaiser, H. F. The Application of Electronic Computers to Factor Analysis. Educ. Psychol. Meas. 20, 141–151, https://doi.org/10.1177/ 001316446002000116 (1960).

- Vol, N. Principal Component Analysis (2nd ed) (Book). J. Am. Stat. Assoc.
  1082–1083. https://doi.org/10.2307/30045356 (2003), page.
- Gollisch, T. & Meister, M. Eye Smarter than Scientists Believed: Neural Computations in Circuits of the Retina. *Neuron* 65, 150–164, https://doi.org/10.1016/j.neuron.2009.12.009 (2010).
- 37. Liu X. L., Yin Z. Q., Yuan Y. S. "Visual neurophysiology," (People's Medical Publishing House 600, 2011).
- 38. Gazzaniga, M. S., Ivry, R. B. & Mangun, G. R. Cognitive neuroscience: the biology of the Mind. *Q. Rev. Biol.* (2002).
- Feng, Y. Q. et al. Performance prediction and optimization of an organic Rankine cycle (ORC) for waste heat recovery using back propagation neural network. *Energy Convers. Manag.* 226, 113552. https://doi.org/10.1016/j.enconman.2020.113552 (2020).
- 40. Govindaraju, R. S. Artificial neural networks in hydrology. I: preliminary concepts. *J. Hydrol. Eng.* **5**, 115–123 (2000).
- Govindaraju, R. S. Artificial neural networks in hydrology. II: hydrologic applications. J. Hydrol. Eng. 5, 124–137 (2000).
- Dang, R., Guo, W., Luo, T. Correlated colour temperature index of lighting source for polychrome artworks in museums. *Build. Environ*. 185 https://doi.org/10.1016/j.buildenv.2020.107287 (2020).
- Royer, M. P. Tutorial: background and guidance for using the ANSI/ IES TM-30 method for evaluating light source color rendition. LEUKOS 18, 191–231 (2021).
- Ghasemi, A. & Zahediasl, S. Normality tests for statistical analysis: a guide for non statisticians. *Int. J. Endocrinol. Metab.* 10, 486–489 (2012).
- 45. Albaum, G., Best, R. & Hawkins, D. Continuous vs discrete semantic differential rating scales. *Psychol. Rep.* **49**, 83–86 (1981).
- Khanh, T., Bodrogi, P., Guo, X., Vinh, Q. & Fischer, S. Colour preference, naturalness, vividness and colour quality metrics, part 5: a colour preference experiment at 2000 lx in a real room. *Light. Res. Technol.* 51, 262–279, https://doi.org/10.1177/1477153517737133 (2019).
- Wang, Y. et al. Low cycle fatigue life prediction of titanium alloy using genetic algorithm-optimized BP artificial neural network. *Int. J. Fatigue* 172, 107609 (2023).

## Acknowledgements

This research was supported by the National Natural Science Foundation of China (Grant Nos. 52208132), the International Science and Technology Cooperation Program of Henan Province (Grant Nos. 242102521029), the Research Programs of the National Museum of China (Grant Nos. GBKX2024Y38).

## **Author contributions**

All authors have made significant contributions to the present work, and their individual roles are detailed as follows. ZL: methodology, software, validation, writing—original draft preparation. HW: software, validation, visualization. QB: visualization. KX: software. YL: software. LM: visualization. RD: writing—review and editing. All authors read and approved the final manuscript.

## **Competing interests**

The authors declare no competing interests.

#### Additional information

**Correspondence** and requests for materials should be addressed to Rui Dang.

**Reprints and permissions information** is available at http://www.nature.com/reprints

**Publisher's note** Springer Nature remains neutral with regard to jurisdictional claims in published maps and institutional affiliations.

Open Access This article is licensed under a Creative Commons Attribution-NonCommercial-NoDerivatives 4.0 International License, which permits any non-commercial use, sharing, distribution and reproduction in any medium or format, as long as you give appropriate credit to the original author(s) and the source, provide a link to the Creative Commons licence, and indicate if you modified the licensed material. You do not have permission under this licence to share adapted material derived from this article or parts of it. The images or other third party material in this article are included in the article's Creative Commons licence, unless indicated otherwise in a credit line to the material. If material is not included in the article's Creative Commons licence and your intended use is not permitted by statutory regulation or exceeds the permitted use, you will need to obtain permission directly from the copyright holder. To view a copy of this licence, visit <a href="https://creativecommons.org/licenses/by-nc-nd/4.0/">https://creativecommons.org/licenses/by-nc-nd/4.0/</a>.

© The Author(s) 2025